


## PAPER

[View Article Online](#)  
[View Journal](#) | [View Issue](#)Cite this: *Nanoscale*, 2021, **13**, 3010

# A high-voltage quasi-solid-state flexible supercapacitor with a wide operational temperature range based on a low-cost “water-in-salt” hydrogel electrolyte†

Yongqi Deng, Hongfei Wang, Kefu Zhang, Jingwen Shao, Jun Qiu, Juan Wu, Yihan Wu and Lifeng Yan \*

Recently, “water-in-salt” electrolytes have provided a huge boost to the realization of high energy density for water-based supercapacitors by broadening the electrochemical stability window. However, the high cost and low conductivity of high concentration LiTFSI greatly restrict the possibility of practical application. Herein, we adopt a new strategy to develop a low-cost and quasi-solid-state polyelectrolyte hydrogel accommodating a superhigh concentration of CH<sub>3</sub>COOK through *in situ* polymerization, avoiding the problem that many conventional polymers cannot accommodate ultra-high ion concentration. The polyelectrolyte hydrogel with 24 M CH<sub>3</sub>COOK exhibits a conductivity of up to 35.8 mS cm<sup>−1</sup> and a stretchability of 950%. With advanced N-doped graphene hydrogel electrodes, the assembled supercapacitor yields a voltage window of 2.1 V with an energy density of 33.0 W h kg<sup>−1</sup> and superior cyclability with 88.2% capacitance retention at 4 A g<sup>−1</sup> after 6000 cycles comparable to those supercapacitors using high-cost LiTFSI salts. Besides, the supercapacitor with excellent temperature stability in the range of −20 to 70 °C can light an LED for more than one minute. The assembled flexible device with the PAAK/CMC-24 M gel film sandwiched in between demonstrates excellent bendability from 0° to 180° and shows great potential for flexible/wearable electronic devices. Our feasible approach provides a new route for assembling quasi-solid-state flexible high-energy storage devices with “water-in-salt” electrolytes.

Received 27th November 2020,  
Accepted 6th January 2021

DOI: 10.1039/d0nr08437a

[rsc.li/nanoscale](http://rsc.li/nanoscale)

## Introduction

Currently, electrochemical energy storage (EES) has been subjected to higher standards and requirements due to the growing markets of electric vehicles and the rapid development of portable/wearable consumer electronics.<sup>1</sup> Therefore, exploring reliable, practical and high-performance EES has increasingly become the research focus to meet the needs of practical application.<sup>2</sup> One of the most promising energy storage devices is carbon-based supercapacitors, attributed to their low weight and cost, fast charge and discharge ability, high power density, and remarkable cycling stability.<sup>3–5</sup> However, the further utility of carbon-based supercapacitors is commonly restricted by their inherent low energy density,

which hinders their widespread application in many electrical devices.<sup>6–8</sup> Energy density, a decisive parameter used to assess the electrochemical performance of supercapacitors, can be calculated according to the formula:  $E = 1/2CV^2$ , where  $E$ ,  $C$ , and  $V$  represent the energy density, electrode capacity, and operation voltage window, respectively.<sup>9</sup> Obviously, increasing  $C$  and  $V$  at the same time is a very effective approach to enhance the energy density. The method of designing advanced carbon electrodes has shown feasibility and success, such as heteroatom doping and KOH activation.<sup>3,10</sup> In addition to electrode design, another option worth noting is the optimization of high-voltage window electrolytes.<sup>11,12</sup> Commonly used aqueous electrolytes tend to undergo water decomposition beyond 1.23 V, but they possess many merits such as low cost, non-volatility and high ionic conductivity superior to that of organic electrolytes and ionic liquids.<sup>13</sup> Moreover, complicated and ultra-dry fabrication processes are not required for water-based supercapacitors, which will further save cost and expand the industrial production of the supercapacitors.<sup>14</sup> “Water-in-salt” (WIS) electrolytes coincidentally satisfy the

CAS Key Laboratory of Soft Matter Chemistry, Hefei National Laboratory for Physical Sciences at the Microscale, and Department of Chemical Physics, iCHEM, University of Science and Technology of China, China. E-mail: [lfyan@ustc.edu.cn](mailto:lfyan@ustc.edu.cn)

†Electronic supplementary information (ESI) available. See DOI: 10.1039/d0nr08437a

requirement for high-voltage window and retain the advantages of water-based electrolytes, which are considered as the best candidate.

“Water-in-salt” (WIS) electrolytes are constructed by dissolving a large amount of salt in water so that the mass or volume ratio of salt to the water exceeds.<sup>1</sup> A superhigh concentration salt can effectively suppress the activity of water and widen the electrochemical stability window beyond 3.0 V. Wang and his co-workers first began to dissolve 21 mol LiTFSI, producing an ultra-high concentration aqueous electrolyte for 3.0 V Li-ion batteries successfully.<sup>15</sup> High concentration Li-ions completely bind free water to form solvent sheath structures so that the water molecules are no longer “free”, resulting in the oxygen evolution reaction (OER) and the hydrogen evolution reaction (HER) pushed beyond their thermodynamic potential.<sup>16</sup> Xiao *et al.* utilized the LiTFSI WIS electrolyte to construct 2.2 V symmetric supercapacitors with a maximum energy density of 29.6 W h kg<sup>-1</sup>.<sup>17</sup> Nevertheless, the 21 mol LiTFSI electrolyte loses the advantages of high ionic conductivity of water-based electrolytes and incurs high costs and viscosity, which is not realistic in practical application.<sup>11</sup> More recently, Yan's group introduced acetonitrile into LiTFSI WIS to reduce its viscosity and achieved a 2.2 V high voltage carbon-based supercapacitor with markedly improved rate performance.<sup>18</sup> However, the high cost remains to be addressed, and using a low-cost salt is a viable option. Low-cost and fluorine-free water-in-salt electrolytes such as NaClO<sub>4</sub>,<sup>13</sup> CH<sub>3</sub>COOK,<sup>19–21</sup> NaNO<sub>3</sub>,<sup>22</sup> have also been reported and electrochemical storage devices using these low-cost salts exhibit unexpected electrochemical performance.

Embedding a WIS electrolyte into a suitable hydrogel substrate can not only maintain its broadened voltage window but also avoid potential leakage demerit, thus reducing packaging complexity and cost.<sup>23–26</sup> Dai *et al.* immersed a three-dimensional CS/PAAm composite hydrogel in 10 M LiTFSI solution, and the ionic conductivity of the hydrogel electrolyte was increased by 5 times compared with the bulk solution, and the electrochemical stability window was widened to 2.6 V.<sup>25</sup> The hydrophilic groups in the polymer can also bind to water molecules, and play a synergistic effect with the LiTFSI to further inhibit free water activity.<sup>27</sup> But, to make electrolyte fully penetrate the three-dimensional network in a short time, a more feasible approach is worth uncovering. However, ordinary polymers cannot hold ultra-high concentrations of salt, resulting in the inability to form the polymer hydrogel, or the performance of the obtained hydrogel is not up to the qualified level.<sup>28</sup> Therefore, multifunctional polymer substrates that can accommodate high concentrations of salt are worthy of exploration.

Herein, we designed a novel PAAK/CMC-based interpenetrating polymer network (IPN) polyelectrolyte hydrogel synthesized *in situ* by free radical polymerization. AAK monomer in a CMC (carboxymethyl cellulose) substrate solution was crosslinked by the initiator ammonium persulfate and crosslinker *N,N'*-methylene bisacrylamide. To form hydrogel electrolyte PAAK/CMC-*x* (*x* represents the concentration of CH<sub>3</sub>COOK) in only one step, the double salt of AAK and CH<sub>3</sub>COOK should

exist in the solution at the same time before polymerization. Then AAK can be polymerized to form a polymer substrate at 70 °C, accommodating ultrahigh CH<sub>3</sub>COOK in the solid-state form. Meanwhile, the K<sup>+</sup> in both CH<sub>3</sub>COOK water-in-salt electrolyte and PAAK chains can collectively form solvent-sheath structures with free water and inhibit water activity, thus endowing the PAAK with a dual function. The proposed PAAK/CMC-24 M hydrogel electrolyte exhibits excellent flexibility and a high ionic conductivity of 35.8 mS cm<sup>-1</sup>. Combined with advanced N-doped graphene hydrogel electrodes, an NG//NG all-solid-state water-based supercapacitor using PAAK/CMC-24 M yields a working voltage window of 2.1 V and an unexpected energy density of 33.0 W h kg<sup>-1</sup> with 88.2% of capacitance retention after 6000 cycles. A wide temperature operation range of -20–70 °C was also tested, demonstrating excellent working performance. The assembled flexible device shows fantastic bendability at 0–180°. Such a simple and feasible approach provides a new strategy for preparing WIS hydrogel electrolytes and paves the way for high-performance electrochemical energy storage devices.

## Results and discussion

The preparation of NG hydrogels was based on a simple hydrothermal reaction of GO and urea as shown in Fig. 1a.<sup>29</sup> XPS spectra in Fig. S1a† confirm that N atoms were successfully doped into graphene nanosheets, accounting for nearly 4.6% of atom contents. The high-resolution spectra of N 1s were also analyzed as shown in Fig. S1b,† where three peaks at 398.6, 399.9, and 401.5 eV were assigned to the pyridine-N (N-6), pyrrolic-N (N-5), and quaternary-N (N-Q), respectively. Fig. S2† shows the contact behavior between the NG electrode and high concentration electrolyte. This contact angle (31°) of the NG electrode was much smaller than that of the activated carbon electrode (40°). Compared with commonly used activated carbon electrodes, the N atom-doped graphene electrodes have better wettability to a high concentration electrolyte. Besides, heteroatom-doped carbon materials can also facilitate fast charge transfer and generate extra pseudo capacitance,<sup>3</sup> achieving the effective enhancement of charge storage abilities. Fig. S3† shows the SEM image of NG aerogels, revealing the interconnected porous network with the existence of micropores, mesopores, and macropores. Porous structures provide an accessible pathway and shorten the path for ion transfer, thereby improving charge and discharge efficiency and specific capacitance.

A schematic diagram of the PAAK/CMC-24 M polyelectrolyte hydrogel preparation is shown in Fig. 1b. Firstly, KOH was added in the CMC solution containing an appropriate amount of AA monomer to consume carboxyl groups, to verify the transformation of AA to AAK. Fourier transform infrared spectroscopy (FTIR) was performed to compare the pure PAA, PAAK, and PAAK/CMC hydrogel in the absence of CH<sub>3</sub>COOK salt as shown in Fig. 2a. It can be seen that the band of -COOH disappeared at 1720 cm<sup>-1</sup> and 3500 cm<sup>-1</sup>, instead, the



Fig. 1 The method of NG hydrogel synthesis (a), the schematic diagram of the PAAK/CMC-*x* polyelectrolyte hydrogel preparation (b).

band appeared at  $1431\text{ cm}^{-1}$  and  $1563\text{ cm}^{-1}$  for the PAAK polyelectrolyte hydrogel. This change was attributed to the appearance of carboxylate and the complete transformation of AA to AAK. Moreover, in the PAAK/CMC hydrogel, carboxylate was also present in CMC, and the  $\text{-OH}$  stretching vibration peak at  $3500\text{ cm}^{-1}$  was exactly due to the addition of CMC. Meanwhile, in the PAAK/CMC polyelectrolyte hydrogel, the band of carboxylate underwent a blue shift to  $1425\text{ cm}^{-1}$  and  $1560\text{ cm}^{-1}$  compared to pure PAAK. These shifts indicated the formation of the interpenetrating polymer network (IPN) polyelectrolyte hydrogel between PAAK and CMC chains. To *in situ* form water-in-salt polyelectrolyte hydrogels, a lot of  $\text{CH}_3\text{COOK}$  was added into the as-prepared precursor solution before polymerization of AAK. The obtained PAAK/CMC-24 M hydrogel exhibits a strain of 950%, and the maximum tensile strength is 40 kPa as shown in Fig. 2b. The introduction of CMC significantly enhanced the tensile strength and strain of the polyelectrolyte hydrogel. Digital photos and SEM images of the hydrogel electrolyte are shown in Fig. S4.† It can be seen that the hydrogel can withstand compression and stretching without splintering as shown in Fig. S4a, b and c.† The morphology of the three-dimensional porous network of the PAAK/CMC-water hydrogel was also confirmed as shown in Fig. S4d.† However, the morphological feature of the PAAK/CMC-24 M hydrogel was different because a large amount of salt remained in the three-

dimensional network structure as shown in Fig. S4e.† Fig. S5† further exhibited the stretched state of the polyelectrolyte hydrogel with excellent tensile performance in the universal tensile testing machine.

Linear sweep voltammetry (LSV) tests were performed to measure the electrochemical stability window (ESW) of 24 M  $\text{CH}_3\text{COOK}$ , 30 M  $\text{CH}_3\text{COOK}$ , and PAAK/CMC-24 as shown in Fig. 2c. The electrolyte was employed between two platinum electrodes at a sweep rate of  $10\text{ mV s}^{-1}$  for electrochemical measurements at room temperature. The 24 M  $\text{CH}_3\text{COOK}$ , 30 M  $\text{CH}_3\text{COOK}$ , and PAAK/CMC-24 M exhibited potential windows of 2.5, 2.7, and 3.1 V, respectively.<sup>20</sup> The highly hydrophilic polymer network can inhibit the activity of water and reduce the dynamic decomposition of water molecules, further extending a wider thermodynamic stability window relative to that of an aqueous electrolyte containing 24 M  $\text{CH}_3\text{COOK}$  and 30 M  $\text{CH}_3\text{COOK}$ . Besides, the  $\text{K}^+$  carried by the PAAK/CMC polyelectrolyte hydrogel also played an indispensable role in increasing the electrochemical stability window.

The ionic conductivity of the hydrogel electrolyte was measured by AC impedance in Fig. S6.† The PAAK/CMC-24 M hydrogel exhibited an unexpectedly high ionic conductivity of  $35.8\text{ mS cm}^{-1}$ , which was comparable to the ionic conductivity of 30 M aqueous  $\text{CH}_3\text{COOK}$  ( $31.2\text{ mS cm}^{-1}$ ) and higher than that of 21 M aqueous LiTFSI ( $8.2\text{ mS cm}^{-1}$ ).<sup>15</sup> Compared to the



Fig. 2 FTIR spectra of pure PAA, PAAK and PAAK/CMC hydrogel (a), stress–strain curves of PAAK-24 M and PAAK/CMC-24 M (b), LSV curves at a scan rate of  $10 \text{ mV s}^{-1}$  (c), ionic conductivity of the PAAK/CMC-24 M at a temperature from  $-20$  to  $70^\circ\text{C}$  (d), Raman spectra of PAAK/CMC- $x$  (e). DSC thermograms of pure water and  $24 \text{ M CH}_3\text{COOK}$  in the PAAK/CMC hydrogel (f).

reported literature about hydrogel electrolytes<sup>26,29–33</sup> in Table S1,<sup>†</sup> the PAAK/CMC-24 M hydrogel still showed superior conductivity performance. Fig. 2d presented the temperature-dependent ionic conductivity of the PAAK/CMC-24 M, and  $\log \sigma$  increased with temperature, following the Arrhenius formula from  $-20^\circ\text{C}$  to  $70^\circ\text{C}$ . Even in the environment of  $-20^\circ\text{C}$  in an ice salt bath and  $70^\circ\text{C}$  in the heating plate, the polyelectrolyte hydrogel still showed an excellent ionic conductivity of  $15.4$  and  $70.8 \text{ mS cm}^{-1}$  respectively, indicating appreciable conductivity in harsh environments. It was worth noting that under the approximately same concentration of potassium ions for PAAK/CMC-24 M and  $30 \text{ M CH}_3\text{COOK}$ , there was almost no obvious loss of ion conductivity of the solid electrolyte compared to the aqueous electrolyte. It was most probably bound up with the “jump” mechanism mentioned in the literature where  $\text{K}^+$  cations can move along the charged groups on the polymer backbone.<sup>34</sup> Both polymers of PAAK and CMC in our PAAK/CMC hydrogel network possessed this structure. PAAK/CMC polyelectrolyte hydrogels with different concentrations of  $\text{CH}_3\text{COOK}$  have also been prepared and also exhibited high ionic conductivity as shown in Fig. S7.<sup>†</sup>

Raman spectroscopy shown in Fig. 2e showed that the addition of the water-in-salt electrolyte greatly reduced the activity of free water in the hydrogel. In PAAK/CMC-1 M, most of the water molecules were still in a free state, where O–H stretching vibration gave rise to a broad Raman band, attrib-

uted to various hydrogen-bonding environments in water clusters. However, the peak intensity remarkably reduced in PAAK/CMC-8 M, 16 M, and 24 M due to the formation of water-in-salt electrolytes. DSC experiments were further conducted to investigate the thermal properties of the PAAK/CMC-24 M and PAAK/CMC-water from  $-20^\circ\text{C}$  to  $70^\circ\text{C}$  as shown in Fig. 2f. An obvious thermodynamic transition was observed at  $-5.5^\circ\text{C}$  in PAAK/CMC-water, which deviated greatly from  $0^\circ\text{C}$ . Since in the PAAK/CMC-water hydrogel, the water molecule was almost in a free state, the appearance of the thermodynamic transition peak was inevitable. And the peak shifting to a sub-zero temperature was due to the ionic behavior of the polyelectrolyte hydrogel intrinsically. In contrast, the thermodynamic transition of water molecule in the PAAK/CMC-24 M disappeared, and no obvious corresponding peak appeared near  $0^\circ\text{C}$ . The elimination of the thermodynamic transformation indicated that the existence of the water-in-salt electrolyte can reduce and suppress the mobility and activity of free water in the polyelectrolyte hydrogel.

Fig. S8<sup>†</sup> shows that the assembled NG//NG aqueous supercapacitor with the  $24 \text{ M CH}_3\text{COOK}$  electrolyte achieved an energy density of up to  $23.9 \text{ W h kg}^{-1}$  and a high operating voltage of  $1.9 \text{ V}$ . The excellent performance of the device far exceeded the previously reported supercapacitor with an energy density of  $16.8 \text{ W h kg}^{-1}$  using AC electrodes and the  $30 \text{ M CH}_3\text{COOK}$  electrolyte.<sup>20</sup> Taking into account the



packaging cost and leakage of the electrolyte during practical applications, it is a feasible strategy to *in situ* embed the water-in-salt electrolyte in an appropriate hydrogel. Herein, we further used the N-doped graphene hydrogel as the symmetric electrode and the PAAK/CMC-x polyelectrolyte hydrogel as the solid electrolyte to construct a water-based solid-state hydrogel supercapacitor. As presented in Fig. 3a, the CV curves of PAAK/CMC-x at  $5 \text{ mV s}^{-1}$  were obtained. With the increase of the  $\text{CH}_3\text{COOK}$  concentration in the hydrogel, the operating voltage window also increased, reaching a maximum voltage of 2.1 V when the PAAK/CMC-24 M hydrogel used as the electrolyte. The shape of CV curves of PAAK/CMC-24 M always retained a quasi-rectangle-like geometry until 2.1 V as shown in Fig. S9,<sup>†</sup> which exceeded 0.2 V for the water-based supercapacitor using 24 M aqueous  $\text{CH}_3\text{COOK}$  as the electrolyte. Fig. 3b shows that those CV curves maintained approximate rectangular shapes as the scan rate increased from  $5 \text{ mV s}^{-1}$  to  $100 \text{ mV s}^{-1}$  in the range of 0–2.1 V. When the scan rate reached  $200 \text{ mV s}^{-1}$ , excellent symmetry still remained. As expected, GCD profiles also exhibited a typical triangular shape from  $0.3 \text{ A g}^{-1}$  to  $5 \text{ A g}^{-1}$  as shown in Fig. 3c, demonstrating the ideal EDLC behavior. The solid-state device yielded a high specific capacitance of  $55.1 \text{ F g}^{-1}$  at  $0.3 \text{ A g}^{-1}$  and  $34.3 \text{ F g}^{-1}$  at  $10 \text{ A g}^{-1}$  calculated from the GCD profiles, revealing excellent rate capacity. In addition, there was an extremely low IR drop at the initial stage of the discharge curves which indicate its low resistance. Electrochemical impedance spectroscopy shown in Fig. 3d further demonstrated the equivalent series resistance of  $6.84 \Omega$  and the ion

transport resistance of  $17.28 \Omega$ . Low resistance meant fast ion transfer in the hydrogel electrolyte and was conducive to high-rate charge and discharge.

Moreover, after ten cycles of charging and discharging with different current densities, the supercapacitor still exhibited excellent rate performance and capacitance reversibility as shown in Fig. 4a. The capacitance of  $55 \text{ F g}^{-1}$  at  $0.3 \text{ A g}^{-1}$  was retained after subjecting to  $0.3 \text{ A g}^{-1}$  to  $10 \text{ A g}^{-1}$  over tens of cycles. According to the used electrode area, the areal capacitance of  $154.2 \text{ mF cm}^{-2}$  at  $0.84 \text{ mA cm}^{-2}$  was achieved as shown in Fig. 4b. Noticeably, superior cyclability with 88.2% capacitance retention at  $4 \text{ A g}^{-1}$  and almost 100% coulombic efficiency was maintained during 6000 cycles as shown in Fig. 4c. The Ragone plot shown in Fig. 4d and Table S2<sup>†</sup> manifested a gravimetric energy density of up to  $33.0 \text{ W h kg}^{-1}$  at a power density of  $311.4 \text{ W kg}^{-1}$  comparable to the supercapacitor using LiTFSI,<sup>25,35,36</sup> and superior to those using 17 M  $\text{NaClO}_4$ , 30 M  $\text{CH}_3\text{COOK}$ -based aqueous supercapacitors.<sup>13,20</sup> Benefiting from the high voltage window brought by the water-in-salt electrolyte and the ultra-thin gel electrolyte membrane, high volumetric energy density based on the whole device has been also achieved as shown in Fig. 4e which was higher than that of the reported flexible quasi-solid-state supercapacitor with the low voltage of 0.8 V.<sup>37</sup> The self-discharge curves (SDC) process can be controlled by potential driving at the beginning and 50% voltage drop was governed by the diffusion control.<sup>38</sup> Fig. 4f shows the slower self-discharge rate of PAAK/CMC-24 M than 24 M aqueous  $\text{CH}_3\text{COOK}$  electrolyte.



Fig. 3 Voltage windows of PAAK/CMC-1, 8, 16, 24 M at  $5 \text{ mV s}^{-1}$  (a), CV curves from  $5 \text{ mV s}^{-1}$  to  $200 \text{ mV s}^{-1}$  (b), GCD profiles from  $0.3 \text{ A g}^{-1}$  to  $5 \text{ A g}^{-1}$  (c) and EIS (d) of the NG//NG quasi-solid-state supercapacitor with the PAAK/CMC-24 M polyelectrolyte hydrogel.

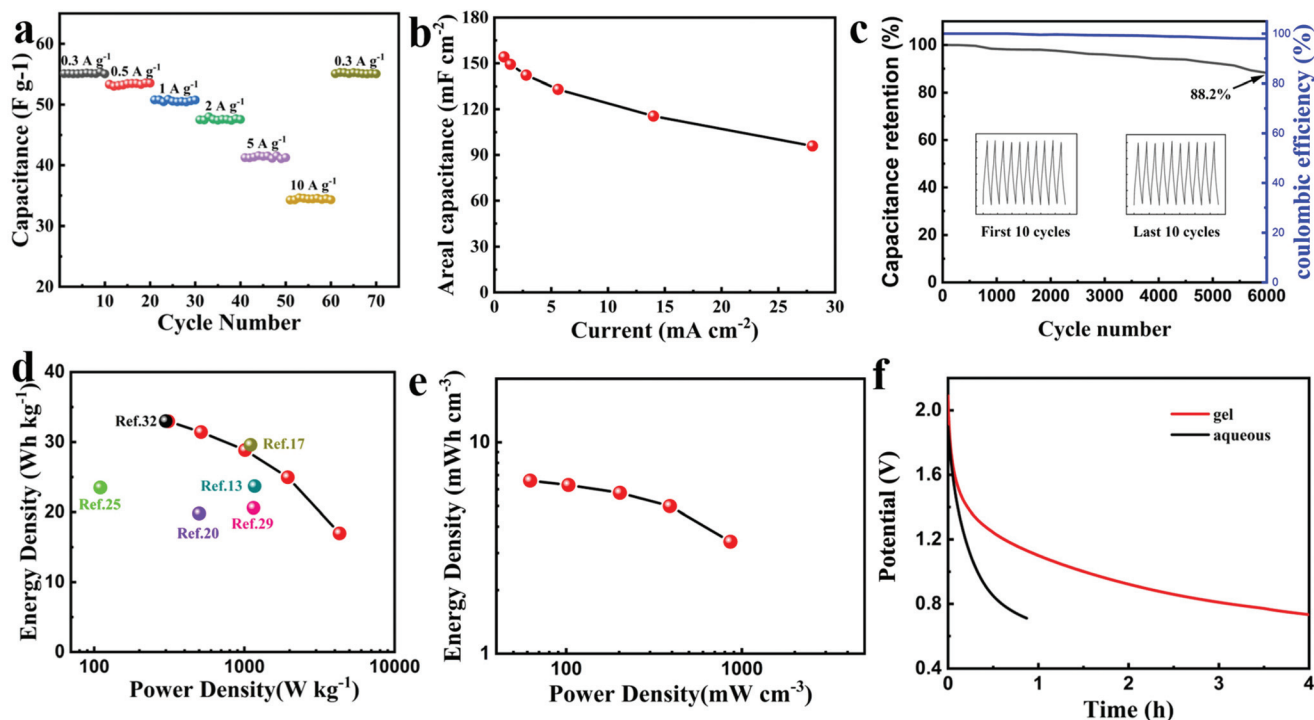


Fig. 4 Electrochemical performances of the NG//NG quasi-solid-state supercapacitor with the PAAK/CMC-24 M polyelectrolyte hydrogel at a voltage of 2.1 V: rate capacity and cycling performance (a), areal capacitance (b), capacitance retention and Coulomb efficiency after 6000 cycles at  $4 \text{ A g}^{-1}$  (c), Ragone plot based on electrode active material (d) and the whole device (e). The self-discharge curves of the NG//NG aqueous 24 M  $\text{CH}_3\text{COOK}$  and hydrogel PAAK/CMC-24 M supercapacitor (f).

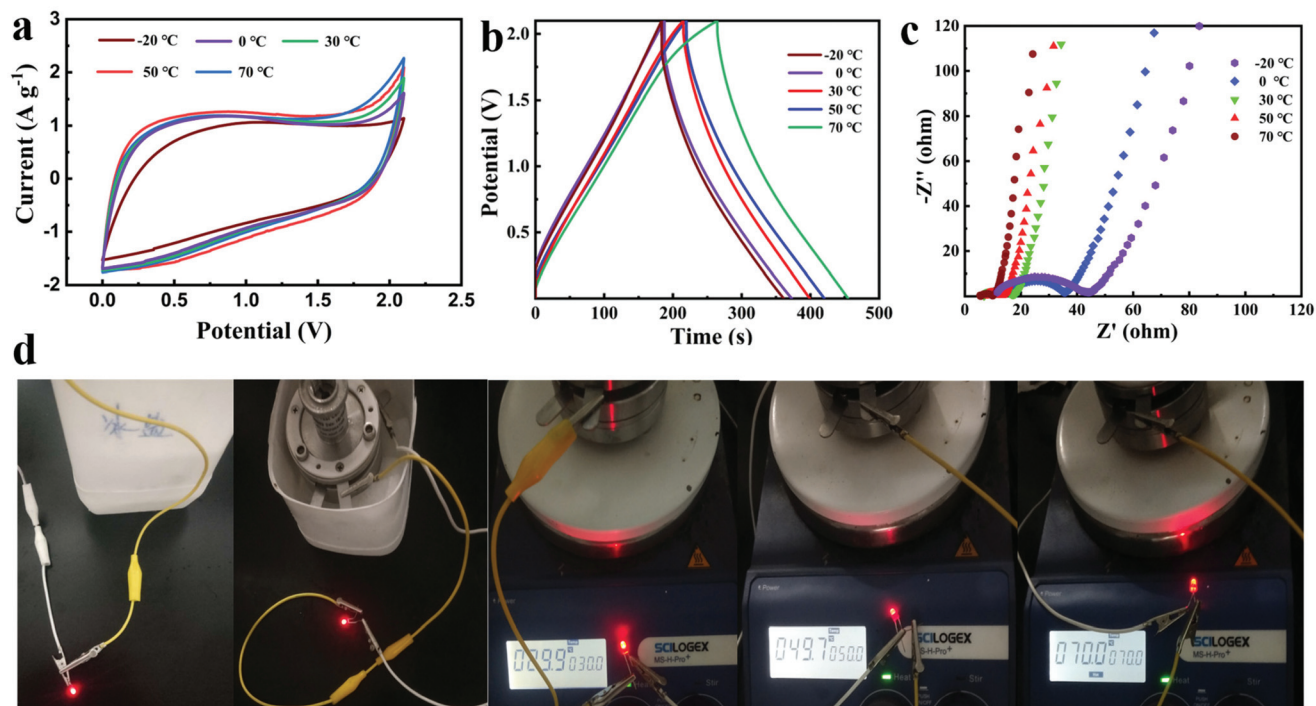


Fig. 5 The NG//NG quasi-solid-state supercapacitor with the PAAK/CMC-24 M polyelectrolyte hydrogel working at different temperatures: CV curves at  $10 \text{ mV s}^{-1}$  (a), GCD curves at  $0.5 \text{ A g}^{-1}$  (b), EIS (c), LED powered (d).

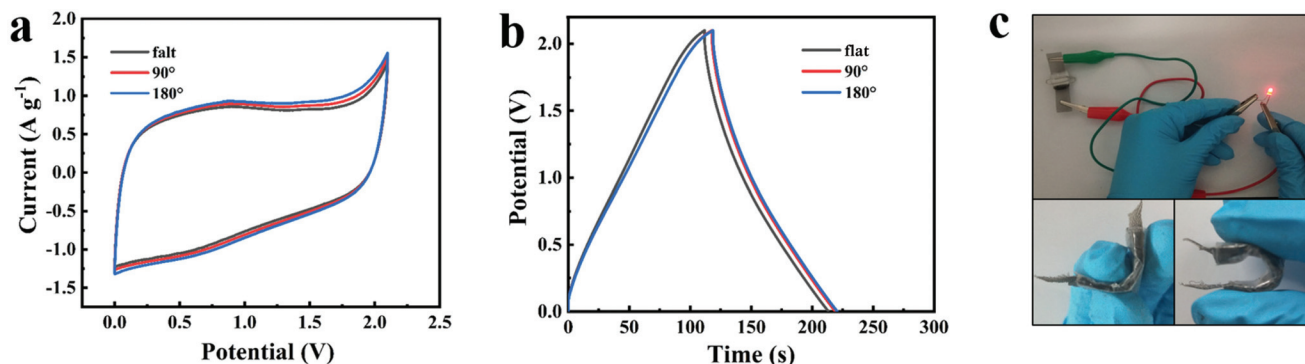


Fig. 6 CV curves at  $10 \text{ mV s}^{-1}$  (a) and GCD profiles at  $1 \text{ A g}^{-1}$  (b) of the assembled flexible device at  $0$ – $180^\circ$ . Optical images of the flexible device under different bending conditions (c).

The temperature adaptability tests of the NG//NG quasi-solid-state supercapacitor with the PAAK/CMC-24 M polyelectrolyte hydrogel were conducted from  $-20^\circ\text{C}$  to  $70^\circ\text{C}$ . Both CV curves and GCD profiles exhibited typical approximate rectangular and triangular shapes as shown in Fig. 5a and b. As the temperature gradually increased from  $-20^\circ\text{C}$  to  $70^\circ\text{C}$ , the enclosed area at  $70^\circ\text{C}$  became larger according to CV curves and GCD profiles, and the capacitance was enhanced by 31% at  $70^\circ\text{C}$  compared to  $-20^\circ\text{C}$ . At high temperatures, due to the increase of liquid fluidity in the hydrogel, the efficiency of ion migration was improved, thus the electric double layer on the electrode surface enriching more charges. In addition, the equivalent series resistance and the ion transport resistance significantly reduced with the increase of temperature as shown in Fig. 5c and Fig. S11,† which also demonstrates that the diffusion and transport of electrolyte ions were promoted. The working status of the device is shown intuitively at different temperatures in Fig. 5d, and an LED could emit light for more than one minute. Benefiting from the excellent mechanical properties of the hydrogel, the CV curves and GCD profiles of the assembled flexible device did not deform and polarise under the different bending conditions as shown in Fig. 6. This indicated the great application potential for flexible and wearable electronic devices.

## Experimental

### Materials

Graphite powder, natural briquetting grade,  $\sim 100$  meshes, 99.9995% (metal basis) was purchased from Alfa Aesar. Analytical grade  $\text{KMnO}_4$ , 98%  $\text{H}_2\text{SO}_4$ , 30%  $\text{H}_2\text{O}_2$ , and 30%  $\text{HCl}$  were purchased from Shanghai Chemical Reagents Company. Analytical grade potassium acetate, acrylic acid, potassium hydroxide,  $N,N'$ -methylene bisacrylamide, and ammonium persulfate were purchased from Sinopharm Group Reagents Company.

### Synthesis of NG hydrogels

Graphene oxide (GO) was prepared according to the modified Hummers' method described in our previous work. Synthesis

of NG hydrogels was achieved by a typical hydrothermal way. In detail, 100 mg of GO in 30 ml of deionized water was dispersed with the aid of mild sonication for 30 min. Next, 1 g of urea was added to the above GO solution and stirred vigorously for 20 min. Finally, the mixed solution of GO and urea was poured in the Teflon-lined stainless steel autoclave at  $180^\circ\text{C}$  for 12 h. Subsequently, the obtained cylindrical NG hydrogel was dialysed against deionized water for 1 day and soaked in anhydrous ethanol over 24 h for use.

### In situ formation of “water-in-salt”-based polyelectrolyte hydrogels

First, 60 mg of CMC was dissolved in 3.8 mL of deionized water under constant stirring at  $80^\circ\text{C}$  until the solution became clear. Next, 1.6 g of AA monomer, 1.34 g of KOH, and 0.016 g of  $N,N'$ -methylene bisacrylamide were added to the above solution at room temperature. After about 30 minutes of full reaction, 9.6 g of potassium acetate was added. Then, potassium acetate was assisted by ultrasound and stirred until the salt was completely dissolved, forming a water-in-salt solution. After that, initiator APS with 1 wt% of AA was added into the solution and stirred for 10 min. Finally, the above solution was transferred to a specific mold and reacted at  $60^\circ\text{C}$  for 3 hours. The obtained hydrogel was denoted as PAAK/CMC-x according to the concentration of  $\text{CH}_3\text{COOK}$ . We also prepared the same gel without CMC, denoted as PAAK-x.

### Assembly of quasi-solid-state supercapacitors and the flexible device

Symmetrical split test cell supercapacitors were assembled with two identical NG hydrogel electrodes using PAAK/CMC-x electrolytes. Two NG hydrogel electrodes pressed into a circular shape (a diameter of 1.2 cm) were fabricated face-to-face with the hydrogel sandwiched between the membrane and electrolyte. The flexible device was constructed by the same method with titanium mesh as a current collector.

### Electrochemical measurements

All electrochemical performance tests were conducted on a CHI660D electrochemical workstation. The ionic conductivity

of electrolytes was conducted using AC impedance tests over a frequency range from 0.1 Hz to 100 k Hz and a voltage amplitude of 5 mV. Two pieces of stainless-steel mesh were placed parallel to each other with the hydrogel sandwiched between them. The electrical conductivity ( $\sigma$ ) was calculated using the following equation:

$$\sigma = \frac{L}{S \times R_b} \quad (1)$$

where  $L$  is the thickness of the hydrogel electrolyte,  $S$  is the contact area of the hydrogel between the electrolyte and electrode,  $R_b$  is the electrical resistance determined by the first point of intersection with the real axis.

Linear sweep voltammetry (LSV) tests were carried out in a two-electrode system to measure the electrochemical stability window (ESW) limits at a scan rate of 10 mV s<sup>-1</sup>. To evaluate the performance of the supercapacitor, cyclic voltammetry (CV), galvanostatic charge-discharge (GCD), and electrical impedance spectroscopy (EIS) were also carried out. Accordingly, the gravimetric capacitance ( $C_g$ ), areal capacitance ( $C_s$ ), gravimetric energy density ( $E_g$ ), areal energy density ( $E_s$ ), volumetric energy density ( $E_v$ ), and power density ( $P$ ) based on the GCD curves were calculated from the following equations:

$$C_g = \frac{I \times V}{t_D \times M} \quad (2)$$

$$C_s = C_g \times \frac{M}{s} \quad (3)$$

$$E_g = \frac{C_g V^2}{2} \quad (4)$$

$$E_s = \frac{C_s V^2}{2} \quad (5)$$

$$E_v = \frac{E_s}{d} \quad (6)$$

$$P = \frac{E \times 3600}{t_D} \quad (7)$$

where  $I$  is the discharge current,  $V$  is the potential window during the discharge process after the IR drop,  $t_D$  is the discharge time,  $s$  is the working area of the electrode and  $d$  is the thickness of the whole device.

### Characterization

To investigate the chemical composition and valence states of NG samples, X-ray photoelectron spectroscopy (XPS) was performed in a Thermo VG Scientific MultiLab ESCA2000 system. The FTIR spectra and Raman spectra were obtained using a Bruker EQUINOX 55 Fourier transform-infrared spectrometer with the KBr disk method and a RAMANLOG 6 (Spex, USA) with an excitation wavelength of 532 nm. The morphology of freeze-dried products was measured using a field emission scanning electron microscope (FESEM, GeminiSEM 500). The wetting behavior and contact angles of aqueous electrolytes were measured employing the Young-Laplace method and a contact angle goniometer VCA2000 (AST Inc.). DSC experi-

ments were performed through TA Instruments Q2000 scanning calorimeter at a heating rate of 5 °C min<sup>-1</sup>. Tensile tests and viscosity tests were performed using a universal testing machine (UTM2502) and Ubbelohde viscometer.

## Conclusions

In summary, the proposed polyelectrolyte hydrogel can accommodate a high concentration of CH<sub>3</sub>COOK and exhibit high ionic conductivity (33.2 mS cm<sup>-1</sup>) with excellent stretchability. The assembled NG//NG quasi-solid-state supercapacitor with PAAK/CMC-24 M achieved a voltage of 2.1 V with an energy density of 33.0 W h kg<sup>-1</sup> and superior cyclability with 88.2% capacitance retention at 4 A g<sup>-1</sup> after 6000 cycles. In addition, the device can power an LED in the temperature range of -20 to 70 °C, indicating excellent environmental adaptability. The assembled flexible supercapacitor can work at 0–180° without sacrificing capacitance. Such an excellent performance exhibited a considerable level with the reported supercapacitors with high-cost LiTFSI salt. The method of using a polyelectrolyte hydrogel to accommodate high concentration ions demonstrated practical feasibility and opens a new avenue to achieve high energy density for electrochemical energy storage with “water-in-salt” electrolytes in the solid-state.

## Conflicts of interest

There are no conflicts to declare.

## Acknowledgements

This work is supported by the National Natural Science Foundation of China (No. 51873201 and 51673180), and the Fundamental Research Funds for the Central Universities (YD2060002015).

## Notes and references

- 1 X. Li, F. Zhang, H. He, J. J. Berry, K. Zhu and T. Xu, *Nature*, 2020, **578**, 555–558.
- 2 F. Wang, X. Wu, X. Yuan, Z. Liu, Y. Zhang, L. Fu, Y. Zhu, Q. Zhou, Y. Wu and W. Huang, *Chem. Soc. Rev.*, 2017, **46**, 6816–6854.
- 3 M. Yang and Z. Zhou, *Adv. Sci.*, 2017, **4**, 1600408–1600418.
- 4 D. Larcher and J. M. Tarascon, *Nat. Chem.*, 2015, **7**, 19–29.
- 5 Z. Yang, J. Ren, Z. Zhang, X. Chen, G. Guan, L. Qiu, Y. Zhang and H. Peng, *Chem. Rev.*, 2015, **115**, 5159–5223.
- 6 M. He, K. Fic, E. Frackowiak, P. Novák and E. J. Berg, *Energy Environ. Sci.*, 2016, **9**, 623–633.
- 7 S. Maiti, A. Pramanik and S. Mahanty, *ACS Appl. Mater. Interfaces*, 2014, **6**, 10754–10762.
- 8 S. T. Senthilkumar, R. K. Selvan, N. Ponpandian, J. S. Melo and Y. S. Lee, *J. Mater. Chem. A*, 2013, **1**, 7913–7919.



- 9 H. Wang, J. Wu, J. Qiu, K. Zhang, J. Shao and L. Yan, *Sustainable Energy Fuels*, 2019, **3**, 3109–3115.
- 10 J. Xu, Z. Tan, W. Zeng, G. Chen, S. Wu, Y. Zhao, K. Ni, Z. Tao, M. Ikram, H. Ji and Y. Zhu, *Adv. Mater.*, 2016, **28**, 5222–5228.
- 11 C. Yang, J. Chen, T. Qing, X. Fan, W. Sun, A. von Cresce, M. S. Ding, O. Borodin, J. Vatamanu, M. A. Schroeder, N. Eidson, C. Wang and K. Xu, *Joule*, 2017, **1**, 122–132.
- 12 X. Fan, L. Chen, O. Borodin, X. Ji, J. Chen, S. Hou, T. Deng, J. Zheng, C. Yang, S. C. Liou, K. Amine, K. Xu and C. Wang, *Nat. Nanotechnol.*, 2018, **13**, 715–722.
- 13 X. Bu, L. Su, Q. Dou, S. Lei and X. Yan, *J. Mater. Chem. A*, 2019, **7**, 7541–7547.
- 14 M. Zhang, S. Makino, D. Mochizuki and W. Sugimoto, *J. Power Sources*, 2018, **396**, 498–505.
- 15 L. Suo, O. Borodin, T. Gao, M. Olguin, J. Ho, X. Fan, C. Luo, C. Wang and K. Xu, *Science*, 2015, **350**, 938–943.
- 16 M. Yu, Y. Lu, H. Zheng and X. Lu, *Chemistry*, 2018, **24**, 3639–3649.
- 17 D. Xiao, Q. Wu, X. Liu, Q. Dou, L. Liu, B. Yang and H. Yu, *ChemElectroChem*, 2019, **6**, 439–443.
- 18 Q. Dou, S. Lei, D.-W. Wang, Q. Zhang, D. Xiao, H. Guo, A. Wang, H. Yang, Y. Li, S. Shi and X. Yan, *Energy Environ. Sci.*, 2018, **11**, 3212–3219.
- 19 S. Wu, S. Hu, Q. Zhang, D. Sun, P. Wu, Y. Tang and H. Wang, *Energy Storage Mater.*, 2020, **31**, 310–317.
- 20 Z. Tian, W. Deng, X. Wang, C. Liu, C. Li, J. Chen, M. Xue, R. Li and F. Pan, *Funct. Mater. Lett.*, 2018, **10**, 1750081–1750085.
- 21 J. Han, H. Zhang, A. Varzi and S. Passerini, *ChemSusChem*, 2018, **11**, 3704–3707.
- 22 J. Guo, Y. Ma, K. Zhao, Y. Wang, B. Yang, J. Cui and X. Yan, *ChemElectroChem*, 2019, **6**, 5433–5438.
- 23 X. Chen, H. Huang, L. Pan, T. Liu and M. Niederberger, *Adv. Mater.*, 2019, **31**, 1904648–1904657.
- 24 Q. Liu, J. Zhou, C. Song, X. Li, Z. Wang, J. Yang, J. Cheng, H. Li and B. Wang, *Energy Storage Mater.*, 2020, **24**, 495–503.
- 25 L. Dai, O. Arcelus, L. Sun, H. Wang, J. Carrasco, H. Zhang, W. Zhang and J. Tang, *J. Mater. Chem. A*, 2019, **7**, 24800–24806.
- 26 L. Liu, Q. Dou, Y. Sun, Y. Lu, Q. Zhang, J. Meng, X. Zhang, S. Shi and X. Yan, *J. Mater. Chem. A*, 2019, **7**, 20398–20404.
- 27 M. Huang, S. Zhen, X. Ren and X. Ju, *J. Power Sources*, 2020, **465**, 228265–228271.
- 28 C. Zhong, Y. Deng, W. Hu, J. Qiao, L. Zhang and J. Zhang, *Chem. Soc. Rev.*, 2015, **44**, 7484–7539.
- 29 H. Wang, Y. Deng, J. Qiu, J. Wu, K. Zhang, J. Shao and L. Yan, *ChemSusChem*, 2020, **13**, 1–11.
- 30 H. Yang, X. Ji, Y. Tan, Y. Liu and F. Ran, *J. Power Sources*, 2019, **441**, 227174–227182.
- 31 R. Na, Y. Liu, N. Lu, S. Zhang, F. Liu and G. Wang, *Chem. Eng. J.*, 2019, **374**, 738–747.
- 32 J. Zhao, J. Gong, G. Wang, K. Zhu, K. Ye, J. Yan and D. Cao, *Chem. Eng. J.*, 2020, **401**, 125456–125462.
- 33 L. Fang, Z. Cai, Z. Ding, T. Chen, J. Zhang, F. Chen, J. Shen, F. Chen, R. Li, X. Zhou and Z. Xie, *ACS Appl. Mater. Interfaces*, 2019, **11**, 21895–21903.
- 34 J. Han, A. Mariani, H. Zhang, M. Zarrabeitia, X. Gao, D. V. Carvalho, A. Varzi and S. Passerini, *Energy Storage Mater.*, 2020, **30**, 196–205.
- 35 Z. Song, H. Duan, D. Zhu, Y. Lv, W. Xiong, T. Cao, L. Li, M. Liu and L. Gan, *J. Mater. Chem. A*, 2019, **7**, 15801–15811.
- 36 S. Wang, J. Qin, Y. Zhao, L. Duan, J. Wang, W. Gao, R. Wang, C. Wang, M. Pal, Z. S. Wu, W. Li and D. Zhao, *ChemSusChem*, 2019, **12**, 3541–3549.
- 37 X. Xiao, X. Peng, H. Jin, T. Li, C. Zhang, B. Gao, B. Hu, K. Huo and J. Zhou, *Adv. Mater.*, 2013, **25**, 5091–5097.
- 38 H. Wang, J. Chen, R. Fan and Y. Wang, *Sustainable Energy Fuels*, 2018, **2**, 2727–2732.